



Gas electrodes with nickel based current collectors for molten carbonate electrolyte thermo-electrochemical cells

Sathiyaraj Kandhasamy , Geir Martin Haarberg , Signe Kjelstrup , Asbjørn Solheim

PII: S2095-4956(19)30237-2
DOI: <https://doi.org/10.1016/j.jechem.2019.05.001>
Reference: JECHEM 851

To appear in: *Journal of Energy Chemistry*

Received date: 21 February 2019
Revised date: 15 April 2019
Accepted date: 2 May 2019

Please cite this article as: Sathiyaraj Kandhasamy , Geir Martin Haarberg , Signe Kjelstrup , Asbjørn Solheim , Gas electrodes with nickel based current collectors for molten carbonate electrolyte thermo-electrochemical cells, *Journal of Energy Chemistry* (2019), doi: <https://doi.org/10.1016/j.jechem.2019.05.001>

This is a PDF file of an unedited manuscript that has been accepted for publication. As a service to our customers we are providing this early version of the manuscript. The manuscript will undergo copyediting, typesetting, and review of the resulting proof before it is published in its final form. Please note that during the production process errors may be discovered which could affect the content, and all legal disclaimers that apply to the journal pertain.

Gas electrodes with nickel based current collectors for molten carbonate electrolyte thermo-electrochemical cells

Sathiyaraj Kandhasamy^{a,*}, Geir Martin Haarberg^a, Signe Kjelstrup^b, Asbjørn Solheim^c

^a *Department of Materials Science and Engineering, Norwegian University of Science and Technology (NTNU), Trondheim, Norway*

^b *PoreLab, Department of Chemistry, NTNU, Trondheim, Norway*

^c *Metal production and processing, SINTEF Industry, SINTEF, Trondheim, Norway*

Abstract

Thermo-electrochemical cells with inexpensive molten carbonate electrolyte and (CO₂|O₂) gas electrodes allow the possible conversion of high temperature waste heat from industrial processes into electricity. The cell containing eutectic (Li,Na)₂CO₃ electrolyte with solid MgO dispersion delivers a large Seebeck coefficient of - 1.7 mV/K. At present, the (CO₂|O₂) gas electrodes use metallic gold as current collectors in order to avoid the formation of interfering oxide layers during operation. For further reduction in energy generation cost, the gold current collectors should be replaced with an inexpensive and stable alternative. In this study, the suitability of the (molten carbonate fuel cell) MCFC's nickel-based cathodes to operate the molten-carbonate thermo-electrochemical cell, was investigated. Ni current collectors were examined in two different states, as NiO and as lithiated NiO (Li_xNi_{1-x}O). The NiO phase shows higher stability than the Li_xNi_{1-x}O while the Seebeck coefficient remains above - 1.2 mV/K.

Keywords: High-temperature thermo-electrochemical cell; Molten carbonate; NiO; Lithiated NiO

* Corresponding author.

E-mail address: k.sathiyaraj14@gmail.com (S. Kandhasamy); Sathiyaraj.kandhasamy@ntnu.no (S. Kandhasamy).

1. Introduction

Waste heat is one of the abundant available renewable energy resources. Almost all the metal producing industry emits a significant amount of waste heat. Especially, in the primary aluminum and silicon producing industries the losses are nearly 50% of the input energy. The emitted waste heat is also at high temperature, in the range of ~ 450 °C for aluminum and ~ 900 °C for silicon production. Thermoelectric generators offer the solution to convert waste heat directly into electricity [1]. However, the stability of semiconductor thermoelectric materials at higher temperatures is unconvincing. Some of the used materials are also expensive and toxic [2,3]. Thermoelectric cells with liquid electrolytes (i.e. thermo-electrochemical cells) have therefore attained consideration as inexpensive cells that perform direct conversion of heat into electricity [4–8]. We will from now on use “thermocell” as a short name, meaning thermo-galvanic or thermo-electrochemical cell. The energy conversion efficiency of the thermocells is small, however. Research on thermocells with aqueous, organic and ionic liquid electrolytes is escalating, but these electrolytes are appropriate only for temperature operation below 200 °C. The valuable waste heat at high temperatures from the metal producing industries should also be addressed.

Recently we have demonstrated a high temperature thermocell using molten carbonate electrolytes with gas electrodes [9–12]. The molten carbonates are comparatively inexpensive, non-toxic, and safe, and they are more stable at higher temperatures than semiconductor thermoelectric materials. So, the recovery of the waste heat at high temperatures is possible [9,10]. Similar high temperature thermocells with molten salt electrolytes are known [13–15]. In some cells, thermal convection in the molten salts may reduce the thermoelectric potential. We found a certain stabilizing effect on the cell potential with dispersion (randomly close-packed) of solid MgO in the molten carbonate electrolyte.

The presence of MgO has a clear impact on the Seebeck coefficient, maybe due to reduction in thermal convection. The Seebeck coefficient with pure Li-carbonate was -0.88 mV/K, while with MgO dispersed in the Li-carbonate it rose to -1.04 mV/K [9]. A chemical reaction between the MgO and CO₂ is possible to favor the MgCO₃ formation. But the large lithium content in the electrolyte and high operating temperature reduces the MgCO₃ formation and retains the MgO phase [9,11,12]. In previous experiments the effective electrolyte composition and gas composition of the electrodes were optimized for enhanced and stable cell operation [9,10,12]. Also the CO₂/O₂ electrode gas flow rate at the three-phase (current collector-gas-electrolyte) interface was studied to establish a well-equilibrated condition for reliable potential reading [11]. Operating conditions were thus partially improved. But metallic gold is still in use as current collector for the gas electrodes to avoid any possible interface reaction (such as oxidization).

The cell potential can be obtained from a series of contributions [9,15,16],

$$\Delta\varphi = \varphi_c - \varphi_a = \Delta_a\varphi + \Delta_{a,e}\varphi + \Delta_e\varphi + \Delta_{e,c}\varphi + \Delta_c\varphi \quad (1)$$

The suffix means the subsystems, anode current collector (a), the two electrode-electrolyte interfaces (a,e and e,c), the electrolyte (e) and the cathode current collector (c). The measured potential ($\Delta\varphi$) is the sum of the potentials contributed by the five different subsystems of the cell (Fig. 1). Dissolution or chemical reaction of the current collectors at the electrode/electrolyte interface may alter the potential contributed by the electrode surfaces ($\Delta_{a,e}\varphi$ and $\Delta_{e,c}\varphi$). In the present context, the gold current collectors are highly stable in molten carbonate giving a small bias potential between the electrodes. However, an inexpensive replacement is needed to cut down power generation cost.

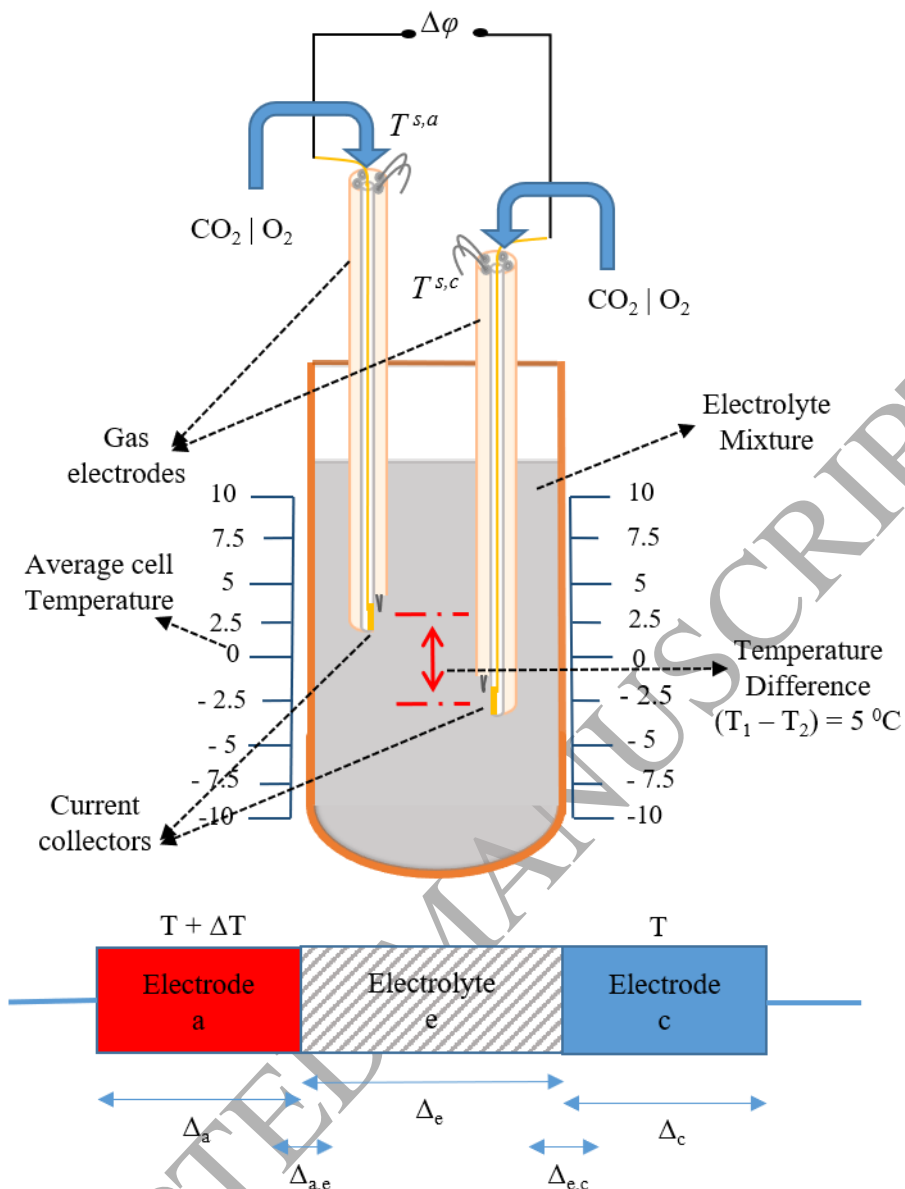


Fig. 1. (Top) Cross-sectional view of the molten carbonate thermo-electrochemical cell and (bottom) the five subsystems of the cell, the notation used for transport properties.

The electrolyte and electrode gas compositions used here are also used in the molten carbonate fuel cell (MCFC) [17,18]. In MCFC, however, oxidized metallic nickel is used for high stability [17,18]. The lithiated NiO (NiO doped with Li) phase displays a better stability in the traditional MCFC with its acidic eutectic $(\text{Li,K})_2\text{CO}_3$ electrolyte. The dissolution rate of lithiated NiO is significantly higher than that of the NiO phase electrode in basic $(\text{Li,Na})_2\text{CO}_3$ electrolyte [17,18]. Even though, we use basic $(\text{Li,Na})_2\text{CO}_3$ with MgO as electrolyte mixture in the thermocell, as a large CO_2 concentration in the electrode gas could

raise the electrolyte acidity [17]. The stability of the NiO phases with and without lithiation is studied. In this manner we investigate the suitability of the nickel-based current collectors for (CO₂|O₂) gas electrodes for molten carbonate thermocells.

2. Experimental

2.1. Materials required

The materials required to fabricate the thermocell were of high purity. Lithium carbonate, sodium carbonate, potassium carbonate and magnesium oxide were purchased from Sigma-Aldrich. Pure gold, platinum and platinum with 10% rhodium (in the form of a wire 0.5 mm diameter) were obtained from K.A. Rasmussen, Norway. A pure nickel sheet of 0.5 mm thickness was obtained from Alfa Aesar. A pre-mixed gas mixture of 34% oxygen and 66% carbon dioxide was from AGA, Norway. Alumina tubes (5 mm outer diameter and 550 mm length) with one center bore of diameter 2.3 mm and four other bores with 0.75 mm diameter and tubular crucible (inner diameter of 38 mm with 200 mm length) were bought from MTC Haldenwanger, Germany.

2.2. Fabrication of current collectors

The current collectors for the gas electrodes were fabricated using gold or nickel sheet (5 × 5 mm) spot-welded to the gold wire. Before the measurements, the fabricated nickel current collectors were oxidized by two different methods (*in-situ* and *ex-situ*). In the *in-situ method*, the nickel current collector was oxidized in the traditional MCFC electrolyte mixture. Here, the carbonates of lithium and potassium were mixed (by hand in a mortar) at eutectic composition and dried in a hot air oven for 48 h at 200 °C. Then, a 90 g sample of the prepared eutectic (Li,K)₂CO₃ was melted at 650 °C for 24 h in a flat-bottomed alumina crucible (Fig. 2) inside a vertical cylindrical furnace under N₂ atmosphere. A pair of Ni

current collectors supported by alumina tubes was inserted into the melt. A separate alumina tube was used to supply the oxidizing gas (66% CO₂ - 34% O₂) mixture at a flow rate of 21 mL/min. The melt temperature was monitored by an S-type thermocouple placed in the electrolyte. This *in-situ* lithiation process was continued for 100 h. Then the oxidizing gas flow was stopped and the metal current collectors were pulled out from the melt. But the metal current collectors were held inside the furnace at 650 °C for 4 h before cooling. In the *ex-situ method*, the nickel current collector was sintered at 700 °C for 4 h and cooled naturally in a tube furnace under synthetic air atmosphere.

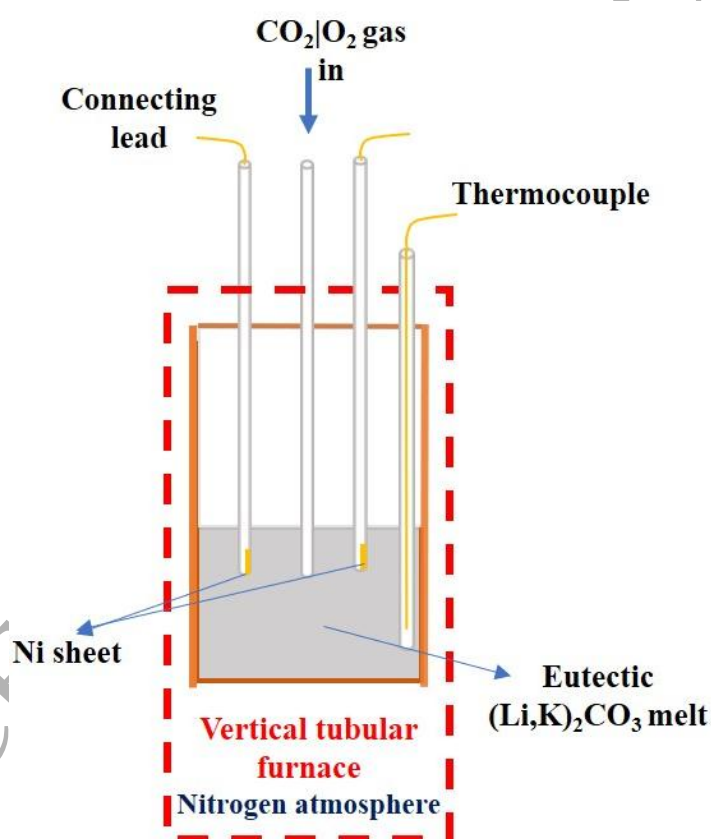


Fig. 2. In cell *In-situ* oxidization of the Ni to attain lithiated NiO current collector.

2.3. Thermocell measurement

The cell (Fig. 1) consisted of an Al₂O₃ tubular crucible, with two electrodes immersed in the molten carbonate electrolyte mixture (~110 g). The electrolyte mixture was prepared by mixing the 45 vol% of eutectic (Li,Na)₂CO₃ and 55 vol% MgO by hand in a mortar. The

mixture was dried for more than 48 h at 200 °C. In each alumina tube, the gold wire lead was inserted into the center bore (diameter 2.3 mm) of a 5-bore Al₂O₃ tube. The thermocouple (Pt-Pt10%Rh) was inserted into two of the other holes (diameter 0.75 mm) and the junction was positioned as near as possible to the current collector. Then the cell was placed inside a standard laboratory vertical tubular furnace. First, the electrolyte was melted under N₂ atmosphere at 550 °C in the vertical tube furnace at least for 48 h. Then the CO₂/O₂ gas was supplied through the bores of the ceramic tube, a pair of Brooks Instrument Sho-Rate meters controlling the flow rate (21 mL/min). The temperature of the electrodes and the cell potential were recorded every 10 sec by using Agilent, 34972A data acquisition unit to determine the Seebeck coefficient, as the ratio of the measured electric potential difference and the temperature difference of the electrodes.

Then the power output of the cell was determined by a direct current (DC) measurement. For the DC measurement, a variable load resistance (R_{ext}) was introduced in parallel to the cell and the measuring unit. The external load resistance was decreased from 10 M Ω to 1 Ω and the corresponding change in potential was recorded after 30 s from the time of the change in each resistance point. Later these measured potentials and the applied known resistance load were used to estimate the current according to Ohm's law and converted into power output. The Seebeck coefficient and power output were determined for cells assembled with different current collectors (gold, NiO and lithiated NiO).

2.4. Physical characterization

The Ni current collectors were subjected to XRD and SEM analysis after different processes, such as the as-purchased Ni, both *in-situ* and *ex-situ* oxidized Ni, and after thermocell potential measurements. For XRD analysis, the samples were mounted over a clay. The XRD phase analysis was performed by using a Bruker-D8 ADVANCE X-ray

diffraction with $\text{CuK}\alpha$ radiation ($\lambda = 1.5406 \text{ \AA}$). The surface morphology of the current collectors was detected by a Hitachi S-3400N Scanning electron microscope (SEM). The samples were fixed on sample supporters (stubs) by a conductive carbon tape. The secondary electrons emitted from the sample surface were detected to picture the surface morphology.

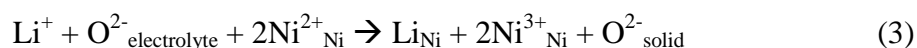
3. Results and discussion

3.1. Structural analysis on oxidized Ni current collectors

In MCFC, Ni oxidization is part of the cell operation, as an in-cell (*in-situ*) process. Once the cell has been brought to the operating temperature (650 °C), Ni oxidization begins [19,20]. To establish similar oxidization conditions in this study, the *in-situ* Ni oxidization was performed in a closed cell containing the molten eutectic $(\text{Li,K})_2\text{CO}_3$ supplied with CO_2/O_2 gas maintained at 650 °C. The Ni metal in contact with O_2 gas and $(\text{Li,K})_2\text{CO}_3$ electrolyte undergoes a stage-by-stage oxidization as time increases, like for instance $\text{Ni} \rightarrow \text{NiO} \rightarrow \text{Li}_x\text{Ni}_{1-x}\text{O}$ (lithiated NiO phase) [21–23]. First, the O_2 gas oxidizes Ni to form NiO by the following reaction [23–25],



Then the resultant NiO in contact with the molten $(\text{Li,K})_2\text{CO}_3$ undergoes further oxidization by the Ni^{2+} to Ni^{3+} transition with subsequent Li^+ (from the electrolyte) insertion as follows,



The time required to achieve the $\text{Li}_x\text{Ni}_{1-x}\text{O}$ -phase and a sufficient content of Li inserted depends on the oxidizing gas composition [24]. A higher ratio of O_2 in the oxidization gas will accelerate the Li_2CO_3 decomposition and increase the amount of Li inserted [26]. If the Li content inserted is greater than 0.4 (i.e. $x > 0.4$), cubic $\text{Li}_x\text{Ni}_{1-x}\text{O}$ changes to hexagonal

LiNiO₂ phase [27]. The LiNiO₂ phase is highly unstable in molten carbonates compared to the cubic Li_xNi_{1-x}O. Therefore, in order to achieve the Li_xNi_{1-x}O phase with ($x < 0.2$), the *in-situ* oxidization is performed with (66% CO₂ - 34% O₂) gas mixture at 650 °C for 100 h [28,29].

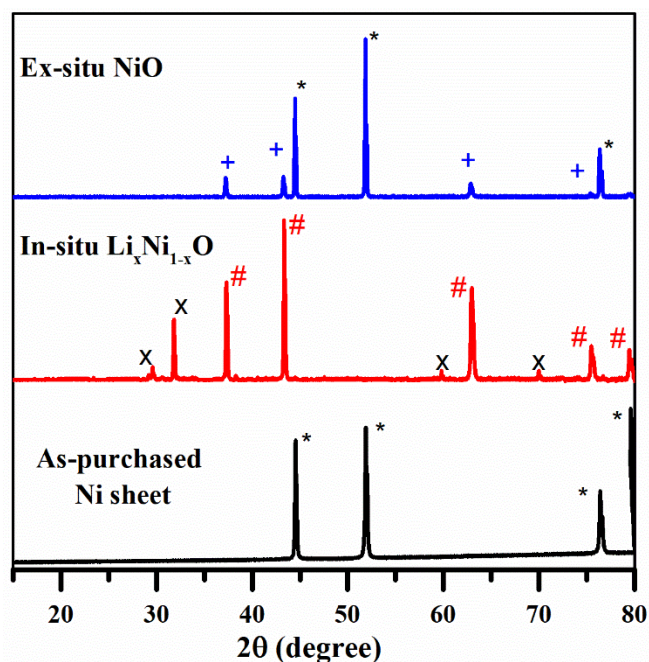


Fig. 3. X-ray diffraction patterns for the Ni current collectors before the thermocell measurements. (JCPDS no.: *00-004-0850 Ni; #04-020-2621 Li_{0.1}Ni_{0.9}O; +01-089-3080 NiO; *01-088-0341 (Li,K)₂CO₃)

The major diffraction pattern (Fig. 3) of the *in-situ* oxidized Ni is coinciding with the Li_{0.1}Ni_{0.9}O phase, and other peaks are matching the phases for (Li,K)₂CO₃. No diffraction peak is observed around 19° (2θ) to support formation of a Li-rich LiNiO₂ phase [25]. The absence of the peaks matching the pure Ni phase, suggests the formation of a thick Li_{0.1}Ni_{0.9}O layer due to oxidization and Li diffusion to few sublayers from the surface. After the *ex-situ* oxidization, Ni phase coexists as a major phase along with NiO. It predicts that in the *ex-situ* process, oxidization occurs just on the surface where Ni is in contact with air; simply as NiO lamination over the Ni, without disturbing the bulk Ni metallic framework [30]. However, no impurity phase is observed, neither after the *in-situ*, nor after the *ex-situ* oxidization processes.

Table 1. Structural parameters obtained from the XRD patterns shown in Fig. 3.

Miller indices (hkl)	<i>In-situ</i> oxidized ($\text{Li}_x\text{Ni}_{1-x}\text{O}$)			<i>Ex-situ</i> oxidized (NiO)		
	2θ (degree)	FWHM (degree)	Relative intensity (%)	2θ (degree)	FWHM (degree)	Relative intensity (%)
111	37.31	0.11	64.53	37.22	0.14	12.95
200	43.34	0.10	100.00	43.26	0.17	13.35
220	62.94	0.19	61.38	62.83	0.21	9.06

Both $\text{Li}_{0.1}\text{Ni}_{0.9}\text{O}$ and NiO phases have cubic structure, thus the peaks appear nearly at the same 2θ positions in Fig. 3. In $\text{Li}_{0.1}\text{Ni}_{0.9}\text{O}$, inserted Li^+ just occupies the vacant cation sites created by oxidization of Ni^{2+} to Ni^{3+} and the cubic structure is maintained. However, the Li^+ insertion can slightly change the unit cell parameter and a corresponding shift in peak positions is expected [25]. Table 1 shows that the $\text{Li}_{0.1}\text{Ni}_{0.9}\text{O}$ diffraction peaks are slightly shifted towards higher 2θ values compared to the NiO diffraction pattern [28]. Also, the $\text{Li}_{0.1}\text{Ni}_{0.9}\text{O}$ peaks are narrow with smaller FWHM (full width at half maximum) compared to the NiO peaks. It confirms that the $\text{Li}_{0.1}\text{Ni}_{0.9}\text{O}$ has attained a higher degree of crystallinity and larger crystallite size than the *ex-situ* oxidized NiO [30].

The SEM surface morphology (Fig. 4) displays that the surface of both of the oxidized Ni is rougher than the pure Ni. An inhomogeneous grain distribution with uneven grain size is observed on the $\text{Li}_{0.1}\text{Ni}_{0.9}\text{O}$ and NiO surfaces. The scale of roughness is smaller in the NiO compared to the $\text{Li}_{0.1}\text{Ni}_{0.9}\text{O}$ surface. Also, large pores like intergranular voids are found on the $\text{Li}_{0.1}\text{Ni}_{0.9}\text{O}$ surface. Probably the recrystallization after Ni oxidization and Li insertion might lead to a lag in interconnection between the grains [19,22,23]. However, no indication of corrosion is observed on the *in-situ* oxidized $\text{Li}_{0.1}\text{Ni}_{0.9}\text{O}$ surface. This confirms that the acid-base equilibrium between Ni and molten $(\text{Li,K})_2\text{CO}_3$ was established by oxidation and lithiation without corroding the metallic Ni.

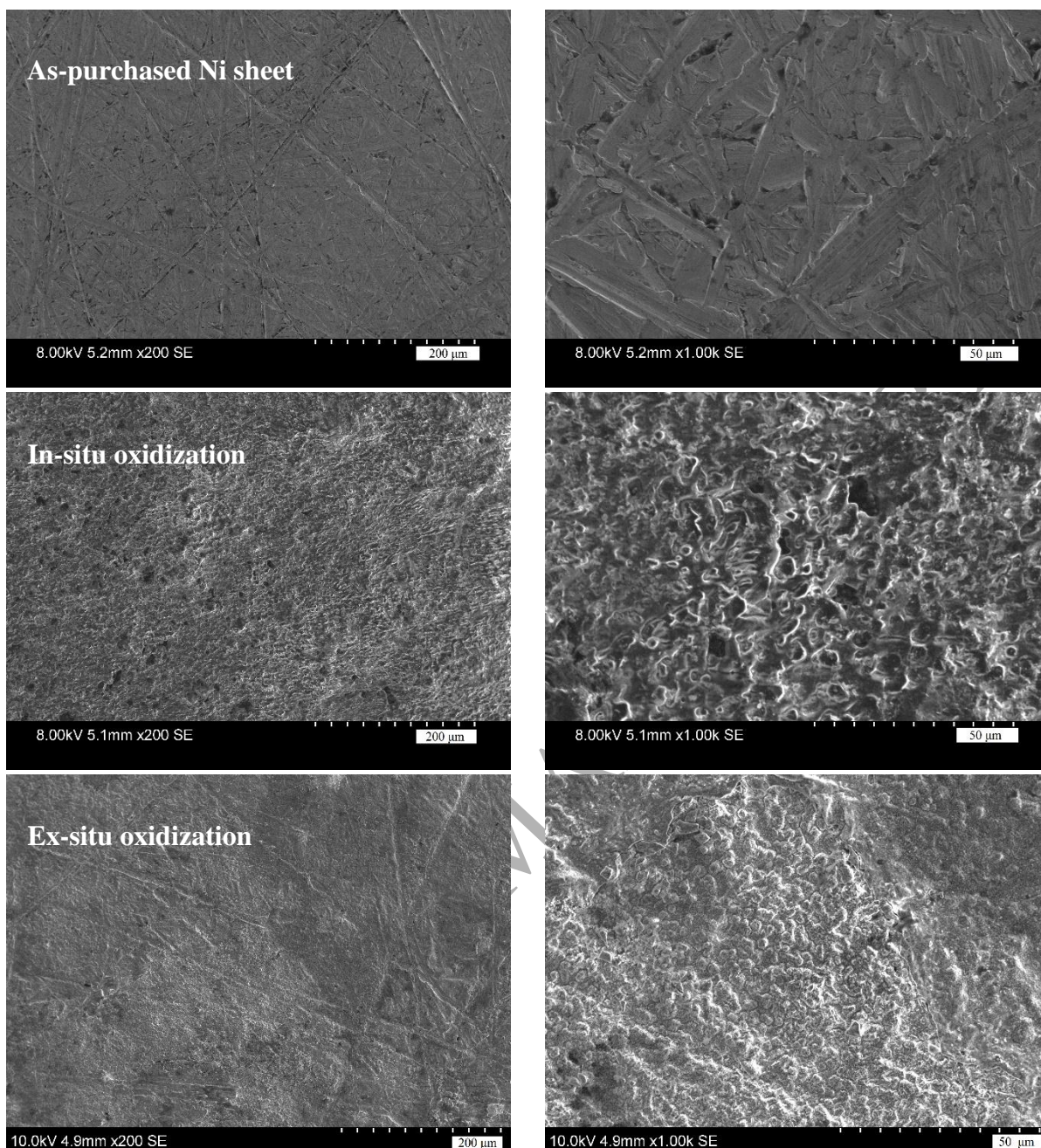


Fig. 4 SEM surface morphology of the Ni current collectors before thermocell measurements (left - low & right - high magnification of the same sample).

3.2. Thermocell measurements with different current collectors

The initial state Seebeck coefficients ($\Delta\phi/\Delta T$) determined from the potential ($\Delta\phi$) measured at short time after establishing the required temperature difference (ΔT) between the electrodes are shown in Table 2. These initial state Seebeck coefficients were measured as reported previously [9–11]. To avoid anomalous thermogalvanic corrosion effect, the electrodes were exposed to a limited set of temperature differences, typically $\sim \Delta T = 10, 0$

and $-10\text{ }^{\circ}\text{C}$. This is because thermogalvanic corrosion could accelerate the chemical reaction and dissolution of the metallic current collector at the electrolyte interface [31]. When both electrodes were held at the average cell temperature ($550\text{ }^{\circ}\text{C}$) to establish $\Delta T = \sim 0\text{ }^{\circ}\text{C}$, a negligible bias potential was observed for all experiments. This confirms the equality of the two electrodes in the cell. The electrodes were the same because both the *in-situ* and *ex-situ* oxidization processes were evenly performed with a couple Ni current collectors.

Table 2. Thermocell measurements with different current collectors in the gas electrodes.

Electrolyte mixture	Current collector	Initial state Seebeck	Power density	Cell
		coefficient (mV/K)	P_{\max}/A ($\mu\text{W}/\text{m}^2$)	resistance (k Ω)
45 vol% eutectic $(\text{Li},\text{Na})_2\text{CO}_3$ with 55 vol% MgO	Au	-1.7 ± 0.04	70.2244	40
	$\text{Li}_{0.1}\text{Ni}_{0.9}\text{O}$	-1.4 ± 0.03	22.4400	100
	NiO	-1.2 ± 0.03	4.1603	800

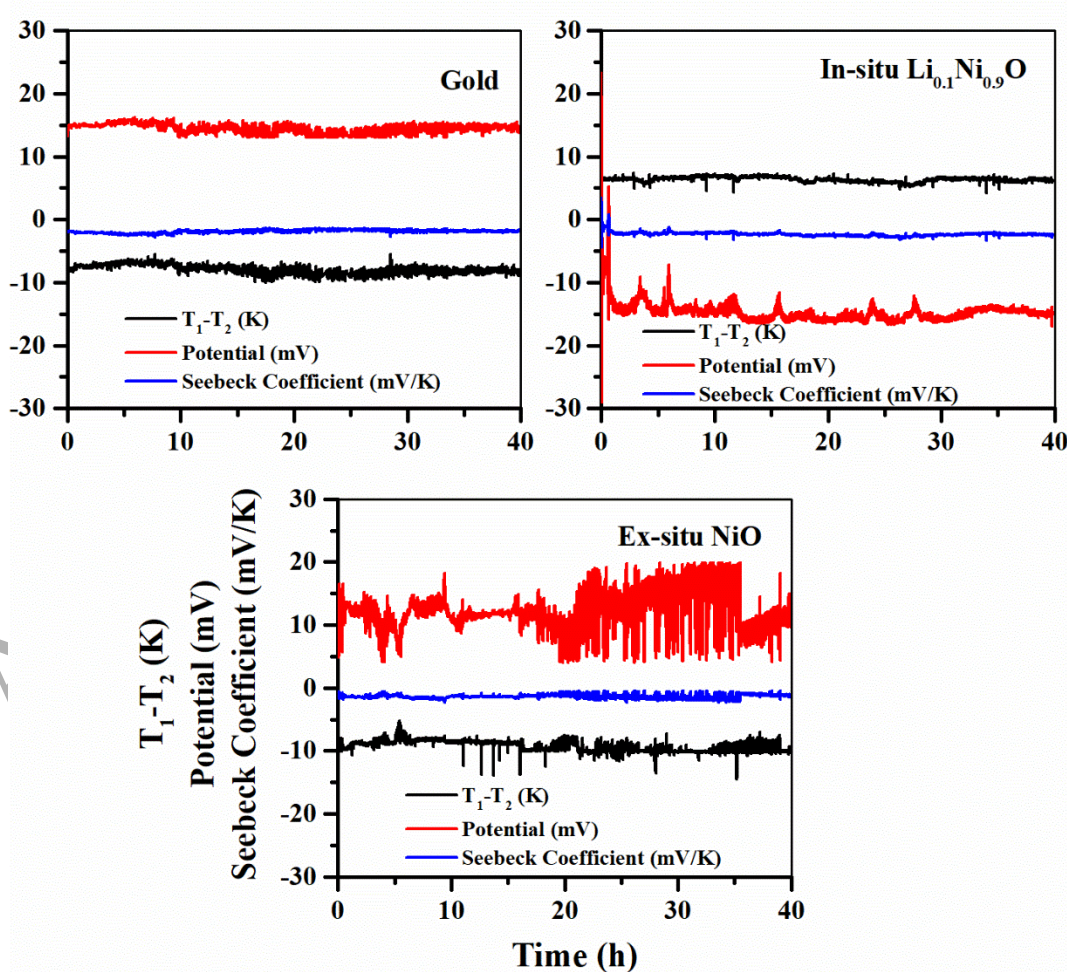


Fig. 5. Seebeck coefficient measurement as a function of time.

Results from long-term measurements (ΔT , $\Delta\phi$ and $\Delta\phi/\Delta T$) of the cells are shown in Fig. 5 as a function of time. Ionic inter-diffusion in the electrolyte mixture takes place and reaches a steady concentration gradient at the so-called Soret equilibrium. It may take several days to reach this steady state [32]. Also, the potential at Soret equilibrium will differ from the initial state potential. A slight potential shift, observed with the stable gold current collector, may be due to onset of the Soret effect rather than of any interface reaction [11]. But the potential drifts are significant for the cells with NiO and $\text{Li}_{0.1}\text{Ni}_{0.9}\text{O}$ current collectors. It shows the possible existence of other chemical reactions at the current collector surface. This will be discussed later.

In the meantime, no pronounced difference in ΔT is observed, irrespective of the current collector material. This is because the stability of ΔT between the electrodes depends on the heat flux in the electrolyte. The present electrolyte composition with the dense dispersion of solid MgO reduces the heat flux in the molten $(\text{Li,Na})_2\text{CO}_3$ [33]. The slight instability observed in ΔT with NiO may be due to dissolution of the hot electrode. It is possible that these NiO particles could move towards the cold electrode (high to low temperature) and affect the ΔT . A similar drift by the corroded particles from high to low energy region is obvious in MCFC and molten salt thermocells with metal electrodes [14,18].

Fig. 6 shows the direct current (DC) measurements of the cells. The maximum of the semicircle provides the possible maximum power output of the thermocell [4]. The cell resistance is determined from the potential vs. current density plot, and the applied external resistance is set equal to the cell resistance at half of the OCP [4]. The determined maximum power output density and resistance of the cells are shown in Table 2. It is well-known that the gold has lower electrical resistance than Ni-based current collectors. In traditional MCFC, along with improved stability the lithiated NiO phase shows a decrease in electrical resistivity

[34]. Electrical resistivity of the current collectors has an impact on the cell potential (Eq. 1), Seebeck coefficients and the power output density [35]. However, the Seebeck coefficients are still above -1.2 mV/K (more negative) with the NiO current collector. The potential vs. current density is linear (Fig. 6) with gold and $\text{Li}_{0.1}\text{Ni}_{0.9}\text{O}$, but non-linear (non-ohmic) behavior was detected with NiO. The cell with NiO illustrated a significant change in the potential (Fig. 5) compared to the $\text{Li}_{0.1}\text{Ni}_{0.9}\text{O}$ with an increase in time. So, a high rate of dissolution is suspected for NiO. But the physical appearance of the current collectors after long-term measurements is reversed. The dimensional loss of $\text{Li}_{0.1}\text{Ni}_{0.9}\text{O}$ is higher than that of NiO. Therefore, both the Ni-based current collectors after long-term measurements were subject to structural analysis.

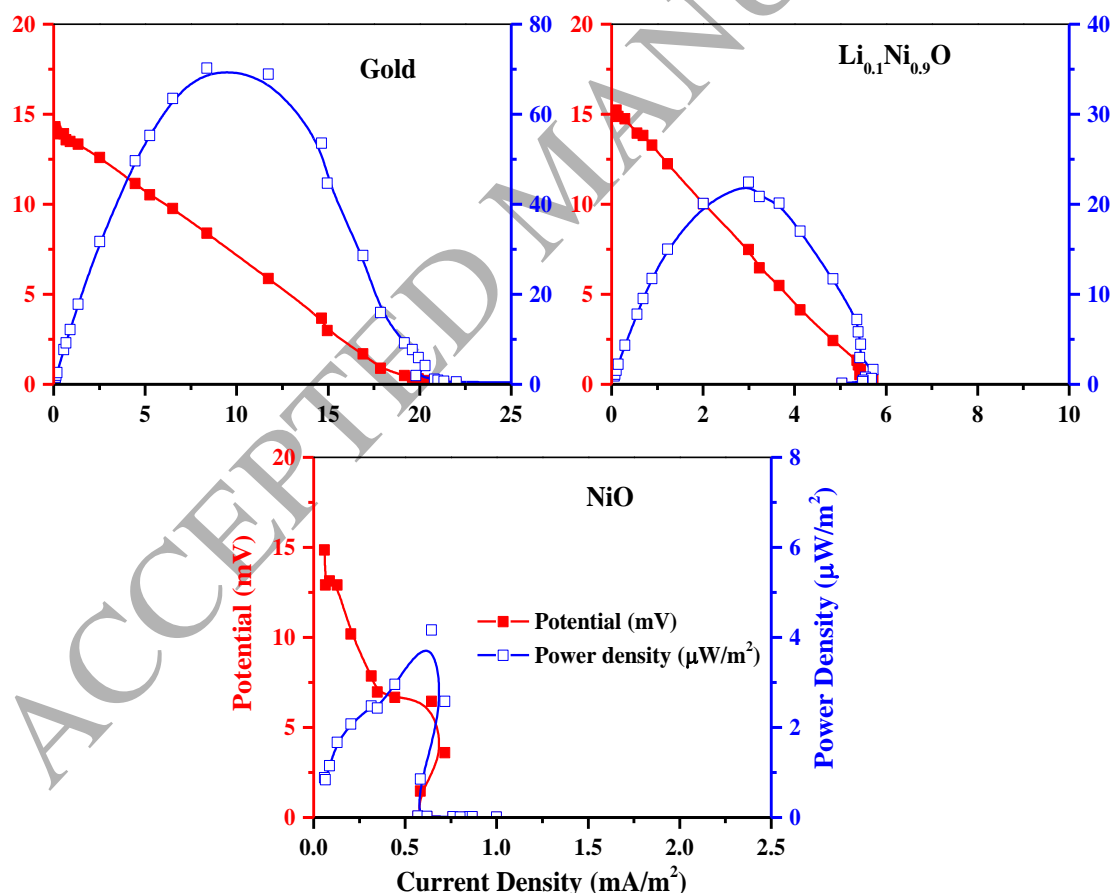


Fig. 6 The direct current measurement to determine the power output density of the cells.

3.3. Structural analysis of Ni current collectors after thermocell measurements

Tables 1 and 3 show a significant variation between the XRD patterns of the current collectors after (Fig. 7) and before (Fig. 3) the thermocell measurements. The relative intensity and the FWHM of the peaks of the specific current collectors differ significantly after 40 h of cell operation, but no additional phases were observed. In $\text{Li}_{0.1}\text{Ni}_{0.9}\text{O}$, the (111) plane becomes predominant and the FWHM is reduced, suggesting that the degree of crystallinity and crystallite size are increased [27]. In the case of NiO, both the relative intensity and the FWHM of the NiO peaks were increased. However, the peak positions (2θ) of the specific current collector before and after are kept in the identical position. It shows that no further lithiation/de-lithiation happened during the thermocell operation [34]. Therefore, the current collectors underwent only phase refinement due to lattice reorientation and change in the degree of crystallinity, such as the sintering effect [30].

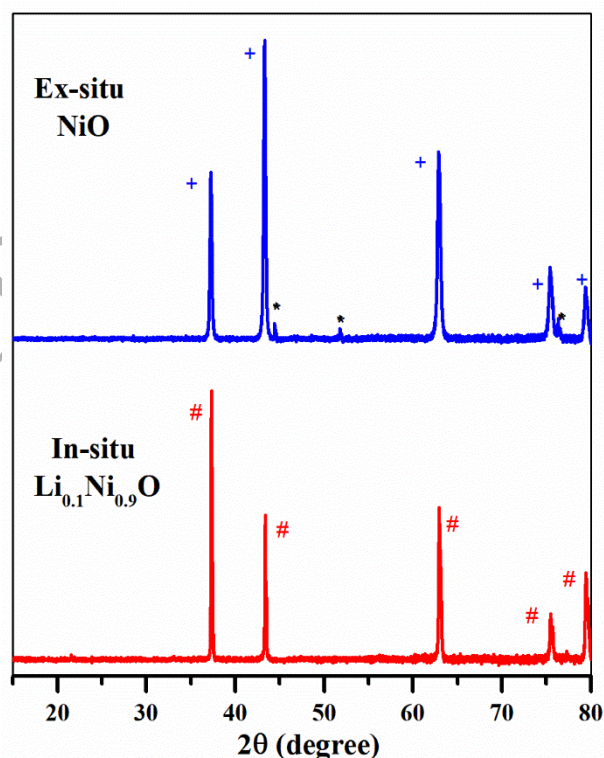


Fig. 7. X-ray diffraction patterns for the Ni current collectors after the thermocell measurements. (JCPDS no.: *00-004-0850 Ni; #04-020-2621 $\text{Li}_{0.1}\text{Ni}_{0.9}\text{O}$; +01-089-3080 NiO)

Table 3. Structural parameters obtained from the XRD patterns shown in Fig. 7.

Miller indices (hkl)	<i>In-situ</i> oxidized ($\text{Li}_x\text{Ni}_{1-x}\text{O}$)			<i>Ex-situ</i> oxidized (NiO)		
	2θ (degree)	FWHM (degree)	Relative intensity (%)	2θ (degree)	FWHM (degree)	Relative intensity (%)
111	37.31	0.10	100.00	37.23	0.21	55.72
200	43.36	0.09	51.93	43.27	0.21	100.00
220	62.92	0.14	57.38	62.86	0.29	64.32

The post SEM analysis (Figs. 8 and 9) shows that the grain size and surface morphology of the current collectors were altered during the cell operation. The large pores found on the $\text{Li}_{0.1}\text{Ni}_{0.9}\text{O}$ (Fig. 4) surface disappeared after the cell operation. Also, the grain size was increased with the formation of some angular shape [34,36]. These grains appear to be as if the Ni is broken into chips and tightly cover the surface on oxidation [27]. On the NiO surface, agglomerated spherical particles with smaller grains than before the thermocell measurement were detected [34,36]. A corrosion effect was detected on the current collector surface after the thermocell measurements and is shown in Fig. 8(b, c, e and f). In the case of $\text{Li}_{0.1}\text{Ni}_{0.9}\text{O}$ a strong corrosion effect was observed at the edges and close to the corroded edges, the lithiated NiO surface layer exposed some cracks. But in NiO, no evidence of corrosion was observed at the edges. However, a few mild pits are found on the surface, like delamination of the pre-made oxide layer [37]. The change in morphology and microstructure of the Ni on the *in-situ* oxidation process to form the $\text{Li}_{0.1}\text{Ni}_{0.9}\text{O}$ could influence the dissolution [30]. The formation of a thick oxide layer, lithiation and intragranular voids may lead to volume expansion and structural weakness (stress and brittle) [19,37]. Thus, a larger dimensional loss is experienced in the $\text{Li}_{0.1}\text{Ni}_{0.9}\text{O}$ than the NiO current collectors [19,30].

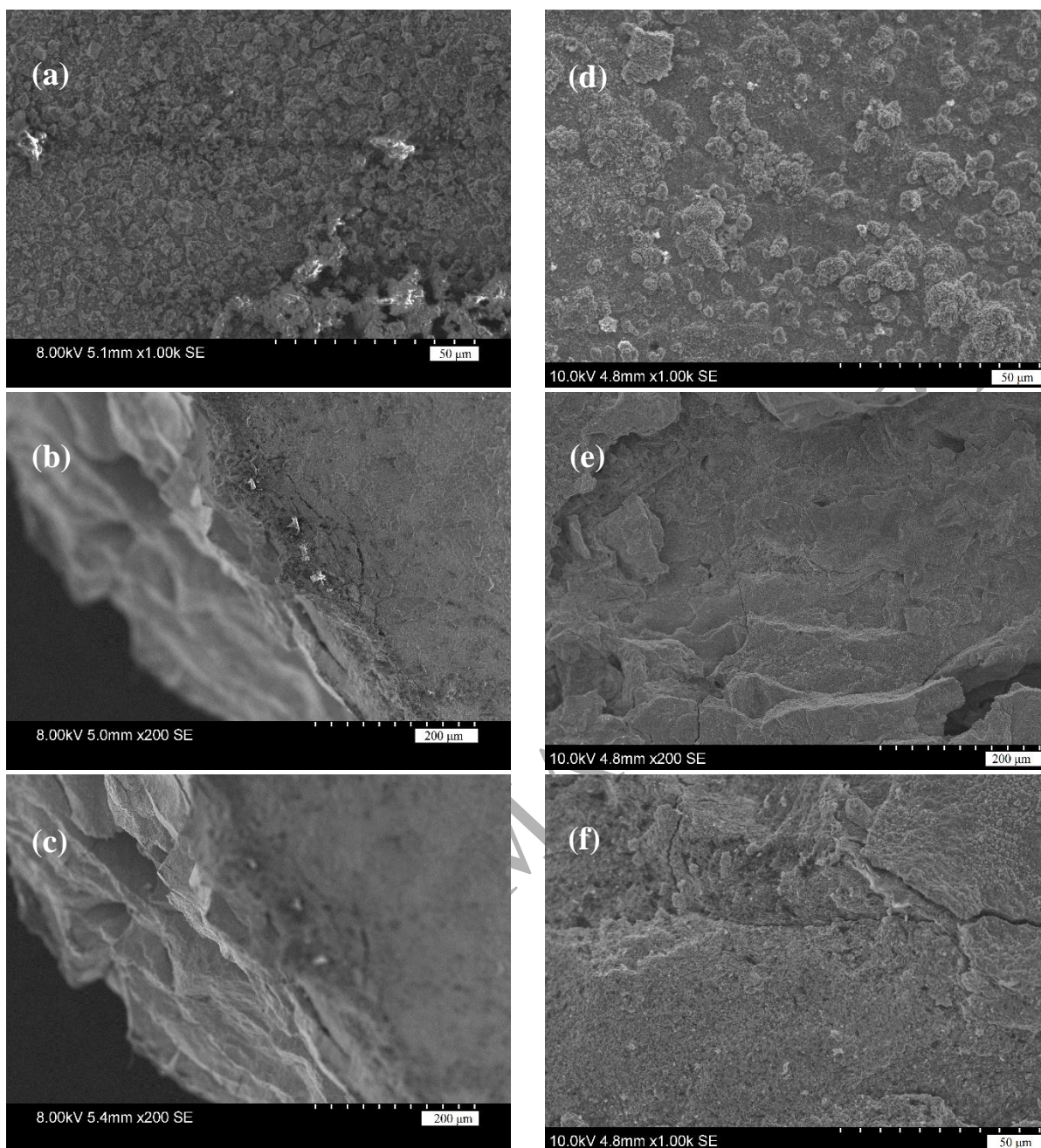


Fig. 8. SEM surface morphology of (a-c) the *in-situ* oxidized $\text{Li}_{0.1}\text{Ni}_{0.9}\text{O}$ and (d-f) the *ex-situ* oxidized NiO current collectors after thermocell measurements.

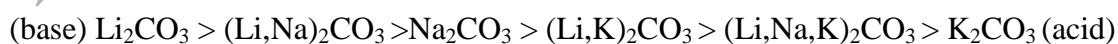
A few mild pits were found on the NiO surface in Fig. 8, like delamination of the pre-made oxide layer [37]. The surface roughness demonstrates that the subsequent Ni layer after delamination was oxidized. This successive oxidization process in molten $(\text{Li,Na})_2\text{CO}_3$ will slow down the NiO dissolution rate and stabilize the NiO after a certain time [30,38]. The increase in relative intensity of the peaks matching the NiO phase in the XRD diffraction

pattern (Fig. 6) after the thermocell operation also supports this understanding. Meanwhile, the existence of minor peaks matching the Ni phase supports the idea that the Ni to NiO transition is still incomplete. The chemical reaction and phase transition are still evident at the NiO current collector and electrolyte interface even after 40 h [39]. This could be a reason for the drift observed in the potential (Fig. 5) and the non-linear potential vs. current density behavior (Fig. 6) for the cell with NiO current collectors even after 40 h. The morphology of the Au current collector (Fig. 9) was not modified during the thermocell operation.



Fig. 9. SEM surface morphology of the gold current collector (a) before and (b) after the thermocell measurements.

In addition to the surface morphology and bulk microstructure, the dissolution will also rely on the acid-base property of the current collector and the electrolyte mixture. NiO is an amphoteric oxide and found to dissolve chemically in both acidic and basic melts. In the case of molten carbonates, the increase in cation size increases the acidity as mentioned below [40],

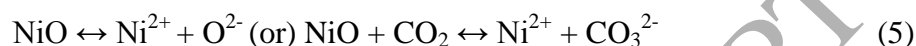


In the cells under investigation, the electrolyte mixture contains 55 vol% basic solid MgO dispersed into the basic $(\text{Li,Na})_2\text{CO}_3$ [40]. Then the basicity of the electrolyte should be

higher than in pure $(\text{Li,Na})_2\text{CO}_3$. So, the following basic dissolution mechanism is expected to take place for NiO in the basic electrolyte [30,40],



If the electrolyte is acidic, the dissolution mechanism of the NiO could be as follows,



The formation of the ion NiO_2^{2-} decreases the amount of NiO dissolved in basic molten $(\text{Li,Na})_2\text{CO}_3$ more than the amount that dissolves in acidic molten $(\text{Li,K})_2\text{CO}_3$ [18,38]. In this regard, the structural stability of the *ex-situ* oxidized NiO current collectors make them into a good replacement for gold. It remains to optimize the electrical conductivity of the NiO phase. Hopefully it can be improved by doping basic metal oxides without losing basicity [18]. Stability of Ni-based electrodes in molten carbonate electrolyte is temperature dependent, and they are highly stable at higher temperatures. Also, the Seebeck coefficient of the thermocells increases with increase in operating temperature. So, increasing the cell operating temperature beyond 550 °C could improve the stability of Ni-based current collector and deliver a larger Seebeck coefficient [27,41].

4. Conclusions

The suitability of inexpensive nickel based current collectors in molten carbonate thermo-electrochemical cells was demonstrated. Such collectors may replace the existing gold as current collector for gas electrodes. The Ni current collector in the NiO phase was obtained by a simple *ex-situ* oxidation process. A high stability in molten $(\text{Li,Na})_2\text{CO}_3$ was shown, and evidenced also by XRD and SEM analysis. The Seebeck coefficient with the NiO current collector remained above - 1.2 mV/K (more negative), but the NiO phase exposed a

high electrical resistivity. Nevertheless, the NiO current collector could be an inexpensive alternative for gold to cut down the energy generation cost with molten carbonate thermocell.

Acknowledgments

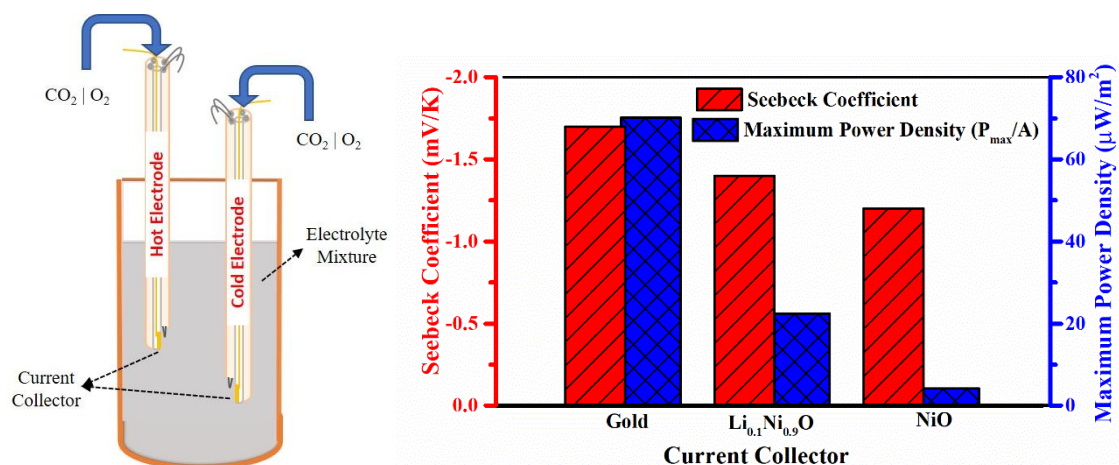
The authors wish to acknowledge the Research Council of Norway for financial support of the research project “Sustainable and Energy Efficient Electrochemical Production and Refining of Metals (SUPREME)” project no. 228296 under the ENERGIX program and the industrial partners Hydro Aluminum, Boliden, Glencore, and Permascand for support. S. Kjelstrup thanks the Research Council of Norway for its Center of Excellence Funding scheme for Porelab, project no. 262644.

References

- [1] S. LeBlanc, *Sustainable Mater. Technol.* 1-2 (2014) 26-35.
- [2] S. LeBlanc, S.K. Yee, M.L. Scullin, C. Dames, K.E. Goodson, *Renewable Sustainable Energy Rev.* 32 (2014) 313-327.
- [3] K. Yazawa, A. Shakouri, *Environ. Sci. Technol.* 45 (2011) 7548-53.
- [4] A. Gunawan, C.-H. Lin, D.A. Buttry, V. Mujica, R.A. Taylor, R.S. Prasher, P.E. Phelan, *Nanoscale Microscale Thermophys. Eng.* 17 (2013) 304-323.
- [5] T.J. Salez, B.T. Huang, M. Rietjens, M. Bonetti, C. Wiertel-Gasquet, M. Roger, C.L. Filomeno, E. Dubois, R. Perzynski, S. Nakamae, *Phys. Chem. Chem. Phys.* 19 (2017) 9409-9416.
- [6] T.J. Abraham, D.R. MacFarlane, J.M. Pringle, *Chem. Commun. (Camb.)* 47 (2011) 6260-2.
- [7] T.J. Abraham, D.R. MacFarlane, R.H. Baughman, L. Jin, N. Li, J.M. Pringle, *Electrochim. Acta* 113 (2013) 87-93.
- [8] M.F. Dupont, D.R. MacFarlane, J.M. Pringle, *Chem. Commun. (Camb.)* 53 (2017) 6288-6302.
- [9] M.T. Børset, X. Kang, O.S. Burheim, G.M. Haarberg, Q. Xu, S. Kjelstrup, *Electrochim. Acta* 182 (2015) 699-706.
- [10] X. Kang, M.T. Børset, O.S. Burheim, G.M. Haarberg, Q. Xu, S. Kjelstrup, *Electrochim. Acta* 182 (2015) 342-350.
- [11] S. Kandhasamy, L. Calandrino, O.S. Burheim, A. Solheim, S. Kjelstrup, G.M. Haarberg, *J. Electrochem. Soc.* 164 (2017) H5271-H5276.

- [12] S. Kandhasamy, A. Solheim, S. Kjelstrup, G.M. Haarberg, *ACS Appl. Energy Mater.* 1 (2018) 5386-5393.
- [13] K. Cornwell, *J. Phys. D: Appl. Phys.* 1 (1968) 173-178.
- [14] K. Cornwell, *J. Phys. D: Appl. Phys.* 5 (1972) 1199-1211.
- [15] B.F. Markov, E.B. Kuzyakin, *Russ. Chem. Rev.* 41 (1972) 250-257.
- [16] B.R. Sundheim, J. Rosenstreich, *J. Phys. Chem.* 63 (1959) 419-422.
- [17] K.-i. Ota, *J. Electrochem. Soc.* 139 (1992) 667-671.
- [18] E. Antolini, *Appl. Energy* 88 (2011) 4274-4293.
- [19] E. Antolini, *J. Power Sources* 40 (1992) 265-270.
- [20] E. Antolini, *J. Mater. Sci.* 35 (2000) 1501-1505.
- [21] M. Mohamedi, Y. Hisamitsu, T. Kudo, T. Itoh, I. Uchida, *J. Solid State Electrochem.* 5 (2001) 538-545.
- [22] Y. Izaki, Y. Mugikura, T. Watanabe, M. Kawase, J.R. Selman, *J. Power Sources* 75 (1998) 236-243.
- [23] M. Yazici, *Solid State Ionics* 124 (1999) 149-160.
- [24] J. Youn, B. Ryu, M. Shin, H. Kang, H. Kim, I. Chang, T. Lee, H. Kwon, *Int. J. Hydrogen Energy* 37 (2012) 19289-19294.
- [25] Z. Li, C. Wang, X. Ma, L. Yuan, J. Sun, *Mater. Chem. Phys.* 91 (2005) 36-39.
- [26] S. Iinou, N. Motohira, N. Kamiya, K.-i. Ota, *Bull. Chem. Soc. Jpn.* 72 (1999) 321-326.
- [27] K. Du, K. Zheng, Z. Chen, H. Zhu, F. Gan, D. Wang, *Electrochim. Acta* 245 (2017) 410-416.
- [28] C. Belhomme, M. Cassir, J. Devynck, G. Gregoire, *J. Mater. Sci.* 35 (2000) 2683-2688.
- [29] T. Wang, D. Mantha, R.G. Reddy, *Sol. Energy Mater. Sol. Cells* 140 (2015) 366-375.
- [30] H.-H. Parkt, C.-I. Jang, H.-S. Shin, K.-T. Lee, *Korean J. Chem. Eng.* 13 (1996) 35-39.
- [31] R. Sánchez-Tovar, M.T. Montañés, J. García-Antón, *Corros. Sci.* 60 (2012) 118-128.
- [32] R. Haase, U. Prüsser, J. Richter, *Ber. Bunsen Ges. Phys. Chem.* 81 (1977) 577-584.
- [33] N. Gokon, D. Nakano, S. Inuta, T. Kodama, *Sol. Energy* 82 (2008) 1145-1153.
- [34] M.J. Escudero, T. Rodrigo, J. Soler, L. Daza, *J. Power Sources* 118 (2003) 23-34.
- [35] H. Im, T. Kim, H. Song, J. Choi, J.S. Park, R. Ovalle-Robles, H.D. Yang, K.D. Kihm, R.H. Baughman, H.H. Lee, T.J. Kang, Y.H. Kim, *Nat. Commun.* 7 (2016) 10600.
- [36] E. Antolini, M. Leonini, V. Massarotti, A. Marini, V. Berbenni, D. Capsoni, *Solid State Ionics* 39 (1990) 251-261.
- [37] J. P. T. Vossen, L. Plomp, J.H.W. Dewit, *J. Electrochem. Soc.* 141 (1994) 3040-3049.
- [38] C.-G. Lee, K. Yamada, T. Nishina, I. Uchida, *J. Power Sources* 62 (1996) 145-147.
- [39] H.A.H. Alzahrani, J.J. Black, D. Goonetilleke, J. Panchompoo, L. Aldous, *Electrochem. Commun.* 58 (2015) 76-79.
- [40] S. Scaccia, S. Frangini, *J. Fuel Cell Sci. Technol.* 3 (2006) 208-212.
- [41] W. Weng, L. Tang, W. Xiao, *J. Energy Chem.* 28 (2019) 128-143.

TOC



Molten carbonate electrolyte thermocells with two identical gas (CO₂|O₂) electrodes shows the possibility to utilize waste heat as a power source. Here we investigated the suitability of nickel-based metallic current collectors for these gas electrodes.

ACCEPTED MANUSCRIPT